Torque Ripple Suppression Technique of High-Frequency Signal Injection Sensorless Control

Hyun-Jun Lee[1], Je-Eok Joo[2], and Young-Doo Yoon[2]
[1] Dept. of Automotive Engineering, Hanyang University, Seoul, Korea
[2] Dept. of Automotive Engineering (Automotive-Computer Convergence), Hanyang University, Seoul, Korea

***Abstract*—The high-frequency (HF) signal injection-based sensorless control injects the voltage signal and estimates the rotor position from the induced HF current. However, the induced HF current causes an HF torque, resulting in torque ripples and acoustic noise. To mitigate these disadvantages, this paper proposes a torque ripple suppression technique of an HF signal injection-based sensorless control. The signal injection angle minimizing the HF torque is found with the proposed HF torque ripple regulator based on the analysis of the HF torque from the induced HF current. The HF torque and acoustic noise can be minimized if the proposed method injects the voltage signal into the determined angle. The proposed method was verified through experiments using an 11 kW IPMSM, and the results proved that HF torque could be minimized with the proposed method.**

***Index Terms*—High-frequency signal injection, signal injection sensorless control, torque ripple suppression.**

I. Introduction

Sensorless drives can be classified into model-based and signal injection-based methods. The model-based sensorless control was proposed in [1]-[2], and the method estimates the rotor speed and position using the voltage and current signals with the motor model. The sensorless control guarantees performance at medium/high speed where the signal is sufficiently large, but the control performance deteriorates at zero/low speed.

The high-frequency (HF) signal injection sensorless control (SISC) was proposed to achieve zero/low-speed sensorless control performance [3]. The method injects an HF sinusoidal voltage signal and estimates the rotor position from the induced HF current, enabling robust sensorless control performance at zero/low speed. In [4], a square-wave signal injection sensorless control was proposed. This method makes the signal processing simpler than the sinusoidal signal injection method, and the position estimation performance is improved using higher frequency signal injection. Due to these advantages, the square-wave signal injection method is preferred.

The zero/low-speed sensorless control performance is achieved using the HF SISC. However, the torque ripples may occur due to the induced HF current, and they cause mechanical vibration and audible noise [5]-[6]; thereby, the applications of the SISC have been restricted.

Many studies have been performed to minimize the torque ripple [7]-[8]. In [7], the electric machine design optimization was proposed. The cogging torque and torque ripple can be minimized using asymmetric barrier design and inverting lamination method. In [8], the rotor pole shape optimizing method was proposed to reduce the torque ripple. In [9], HF torque ripple minimization for SISC of IPMSM was proposed. The minimum HF torque ripple can be achieved by adjusting the signal injection angle.

This paper analyzes the HF torque ripples caused by the induced HF current and proposes the HF torque ripple regulator to suppress the HF torque ripple of the square-wave HF signal injection method. The signal injection angle at which the torque ripple becomes zero is found with the proposed HF torque ripple regulator, where the error signal is the HF torque ripple magnitude. The flux data is required to calculate the HF torque ripple since the motor torque is generated according to the flux and current. The flux saturation model and its identification method proposed in [10]-[12] is exploited in this study. Experiments on 11 kW IPMSM were performed to verify the proposed method. The results showed that the torque ripple from the induced HF current was significantly reduced, and the auditory noise was reduced.

II. Proposed Torque Ripple Suppression Technique

A. Conventional HF SISC [4]

Fig. 1 presents the control block diagram of the square-wave SISC proposed in [4]. There is a current control loop for motor torque control, and the HF voltage reference in the estimated rotor coordinates $\mathbf{v}_{\mathbf{dqsh}}^{\hat{\mathbf{r}}*}$ is added to the output of the current controller, i.e., the fundamental-frequency voltage reference in the estimated rotor coordinates $\mathbf{v}_{\mathbf{dqsf}}^{\hat{\mathbf{r}}*}$. Here, subscripts f and h indicates the fundamental-frequency and the HF components. The measured current in the stationary coordinates includes the fundamental and HF components, and the notch filter is used to decouple each component. The fundamental-frequency current is used for the current control while the HF current is used to extract the position error signal.

The square-wave HF voltage reference is

$$\mathbf{v}_{\mathbf{dqsh}}^{\hat{\mathbf{r}}*}[n] \equiv \begin{bmatrix} v_{dsh}^{\hat{r}*}[n] \\ v_{qsh}^{\hat{r}*}[n] \end{bmatrix} = \begin{bmatrix} V_h * clk[n] \\ 0 \end{bmatrix}, \quad (1)$$

where V_h is the injection voltage magnitude, clk is a clock signal that alternates 1 and -1 at a specific frequency, and n represents an index. Equation (1) indicates that the method injects the square-wave voltage signal into the d-axis in the estimated rotor coordinates.

If the HF voltage is synthesized by the PWM inverter, the HF current induced according to the motor impedance.

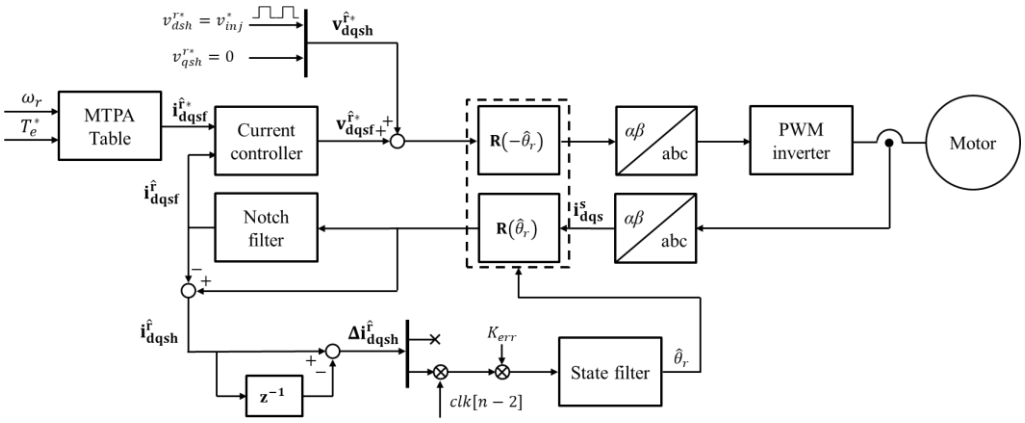

Fig. 1. Block diagram of the square-wave signal injection sensorless control method [4].

The impedance matrix of synchronous motors can be extracted from the machine's voltage model. The voltage model is

$$\mathbf{v_{dqs}^r} \equiv \begin{bmatrix} v_{ds}^r \\ v_{qs}^r \end{bmatrix} = \begin{bmatrix} R_s i_{ds}^r + \frac{d\psi_{ds}^r}{dt} - \omega_r \psi_{qs}^r \\ R_s i_{qs}^r + \frac{d\psi_{qs}^r}{dt} + \omega_r \psi_{ds}^r \end{bmatrix}, \quad (2)$$

where the superscript r indicates the rotor coordinates, v_{ds}^r and v_{qs}^r are the stator voltage, i_{ds}^r and i_{qs}^r are the stator current, ψ_{ds}^r and ψ_{qs}^r are magnetic flux-linkage, R_s is the stator resistance, ω_r is the electrical rotor speed.

If the injection signal frequency ω_h is much greater than the fundamental-frequency ω_r, the machine impedance matrix can be simplified as

$$\mathbf{Z^r} \equiv \begin{bmatrix} R_s + sL_{ds} & -\omega_r L_{qs} \\ \omega_r L_{ds} & R_s + sL_{qs} \end{bmatrix} \approx \begin{bmatrix} sL_{ds} & 0 \\ 0 & sL_{qs} \end{bmatrix} \quad (\omega_h \gg \omega_r). \quad (3)$$

Here, L_{ds} and L_{qs} are self-inductances, and L_{dqs} is the mutual inductance. The mutual inductance is assumed to be small enough ($L_{dqs} \ll 1$) in this method. In this case, the HF voltage model is derived as

$$\mathbf{v_{dqsh}^r}[n-1] = \begin{bmatrix} L_{ds} & 0 \\ 0 & L_{qs} \end{bmatrix} \frac{1}{T_s} \begin{bmatrix} \Delta i_{dsh}^r[n] \\ \Delta i_{qsh}^r[n] \end{bmatrix}, \quad (4)$$

where T_s is a sampling period, and $\mathbf{\Delta i_{dqsh}^r}[n] = \mathbf{i_{dqsh}^r}[n] - \mathbf{i_{dqsh}^r}[n-1]$ is the HF current ripple in the rotor coordinates.

Assuming the most basic single sampling, the voltage reference $\mathbf{v_{dqsh}^{r*}}$ and the actual voltage $\mathbf{v_{dqsh}^r}$ have one sampling delay relationship due to digital delay. This can be expressed as an equation as follows.

$$\mathbf{v_{dqsh}^{r*}}[n-1] = \mathbf{v_{dqsh}^r}[n], \quad (5)$$

Fig. 2 shows the injection voltage signal and the sampled HF current waveforms. The dotted line represents the sampling time point, and $i_{dsh,real}^{\hat{r}}$ is the actual HF current in the estimated rotor coordinates. If the square-wave signal is injected, a triangular-wave current would be induced. Since the q-axis voltage reference in the

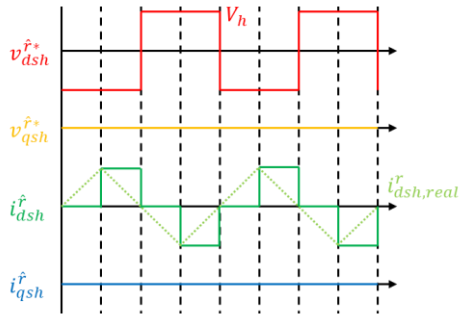

Fig. 2. Injection voltage signal and the sampled high-frequency current waveforms.

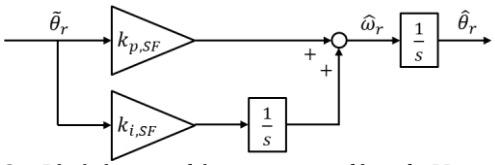

Fig. 3. Block diagram of the position state filter of a PI controller structure.

estimated rotor coordinates is maintained at zero, the induced q-axis current is maintained at zero if there is no position estimation error.

The induced HF current ripple in the rotor coordinates can be calculated using the HF voltage as

$$\mathbf{\Delta i_{dqsh}^r}[n] = \mathbf{Z^{r-1}} \mathbf{R}(\tilde{\theta}_r) \mathbf{v_{dqsh}^{\hat{r}*}}[n-2] T_s, \quad (6)$$

where $\tilde{\theta}_r \equiv \theta_r - \hat{\theta}_r$ is the position estimation error between the rotor angle θ_r and the estimated rotor angle $\hat{\theta}_r$, $\mathbf{R}(\theta) \equiv \begin{bmatrix} \cos\theta & \sin\theta \\ -\sin\theta & \cos\theta \end{bmatrix}$ is the rotating matrix.

In [4], the induced HF current ripple in the estimated rotor coordinates is used to extract the position error signal. The HF current ripple is

$$\mathbf{\Delta i_{dqsh}^{\hat{r}}}[n] = \mathbf{R}(-\tilde{\theta}_r) \mathbf{\Delta i_{dqsh}^r}[n] = V_h T_s * clk[n-2] \begin{bmatrix} \frac{\cos^2\tilde{\theta}_r}{L_{ds}} + \frac{\sin^2\tilde{\theta}_r}{L_{qs}} \\ \frac{(L_{qs}-L_{ds})}{2L_{ds}L_{qs}} \sin(2\tilde{\theta}_r) \end{bmatrix}. \quad (7)$$

The position error signal is extracted from the q-axis HF current ripple in the estimated rotor coordinates as

$$\varepsilon[n] \equiv \tilde{\theta}_r[n]$$
$$\approx \frac{1}{V_h T_s * clk[n-2]} \frac{L_{ds}L_{qs}}{(L_{qs}-L_{ds})} \Delta i^{\hat{r}}_{qsh}[n] \quad (\tilde{\theta}_r \ll 1). \tag{8}$$

The position state filter estimates the rotor speed and position from the error signal, and it can be configured as a proportional-integral (PI) controller structure, as shown in Fig. 3. The transfer function between the actual rotor angle and the estimated rotor angle can be designed as a prototype of the secondary system as

$$\frac{\hat{\theta}_r}{\theta_r} = \frac{k_{p,SF}s + k_{i,SF}}{s^2 + k_{p,SF}s + k_{i,SF}}$$
$$= \frac{2\zeta_{SF}\omega_{n,SF}s + \omega^2_{n,SF}}{s^2 + 2\zeta_{SF}\omega_{n,SF}s + \omega^2_{n,SF}}, \tag{9}$$

where $\omega_{n,SF}$ is the bandwidth, and ζ_{SF} is the damping ratio. The proportional gain $k_{p,SF}$ and the integral gain $k_{i,SF}$ of the state filter for satisfying the above equation are as the following.

$$\begin{cases} k_{p,SF} = 2\zeta_{SF}\omega_{n,SF} \\ k_{i,SF} = \omega^2_{n,SF} \end{cases}. \tag{10}$$

B. HF Torque Analysis

The flux and current have the fundamental-frequency and the HF component if the HF SISC is exploited as

$$\begin{cases} \boldsymbol{\psi}^{\mathbf{r}}_{\mathbf{dqs}} = \boldsymbol{\psi}^{\mathbf{r}}_{\mathbf{dqsf}} + \boldsymbol{\psi}^{\mathbf{r}}_{\mathbf{dqsh}} \\ \mathbf{i}^{\mathbf{r}}_{\mathbf{dqs}} = \mathbf{i}^{\mathbf{r}}_{\mathbf{dqsf}} + \mathbf{i}^{\mathbf{r}}_{\mathbf{dqsh}} \end{cases}. \tag{11}$$

where $\boldsymbol{\psi}^{\mathbf{r}}_{\mathbf{dqs}}$ is the flux-linkage vector.

The entire torque T_e can be divided into the fundamental frequency component T_{ef} and the HF component as

$$T_e = T_{ef} + T_{eh}, \tag{12}$$

where each torque component is

$$T_{ef} = \frac{3}{2}\frac{P}{2}\left(\psi^r_{dsf} i^r_{qsf} - \psi^r_{qsf} i^r_{qsf}\right) \tag{13a}$$

$$T_{eh} = \frac{3}{2}\frac{P}{2}\left(\psi^r_{dsf} i^r_{qsh} - \psi^r_{qsf} i^r_{dsh}\right) + \frac{3}{2}\frac{P}{2}\left(\psi^r_{dsh} i^r_{qsf} - \psi^r_{qsh} i^r_{dsf}\right) + \frac{3}{2}\frac{P}{2}\left(\psi^r_{dsh} i^r_{qsh} - \psi^r_{qsh} i^r_{dsh}\right). \tag{13b}$$

where P is the pole number.

Fig. 4 shows the rotor coordinates flux and current vectors $\boldsymbol{\psi}$ and $\boldsymbol{i}$, including the fundamental frequency and the HF components. The fundamental frequency components of the flux and current vectors ψ_f and i_f are determined according to the current operating point, where each angle is defined as $\theta_{\psi f}$ and θ_{if}. The HF current vector angle θ_{ih} would be zero if the voltage signal is injected into the d-axis, assuming the position error is null. The HF flux vector angle is defined as $\theta_{\psi h}$. Notably, each angle is not the same, and the HF current is represented as

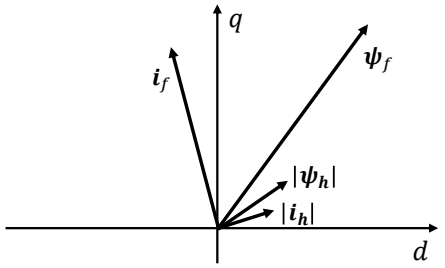

Fig. 4. Flux and current vectors, including the fundamental frequency and high-frequency components.

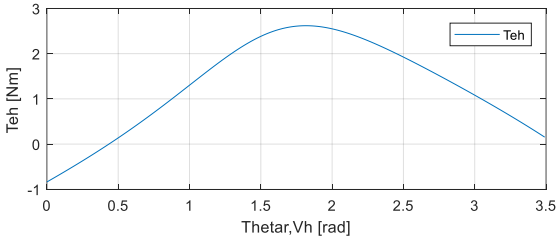

Fig. 5. High-frequency torque ripple according to the voltage signal injection angle.

$$\begin{cases} i^r_{dsh} = sign\left(v^*_{inj}\right) I_h cos\theta_{ih} \\ i^r_{qsh} = sign\left(v^*_{inj}\right) I_h sin\theta_{ih} \end{cases}. \tag{14}$$

where I_h is the magnitude of the HF current vector, $sign\left(v^*_{inj}\right) \in \{-1, 1\}$ is the sign of the injection voltage.

If the HF flux component is small enough ($\boldsymbol{\psi}^{\mathbf{r}}_{\mathbf{dqsh}} \ll \boldsymbol{\psi}^{\mathbf{r}}_{\mathbf{dqsf}}$), the HF torque in (13b) can be simplified using (14) as

$$T_{eh} = \frac{3}{2}\frac{P}{2}\left\{\left(\psi^r_{dsf} + \psi^r_{dsh}\right) sign\left(v^*_{inj}\right) I_h \sin\theta_{Ih}\right\} - \frac{3}{2}\frac{P}{2}\left\{\left(\psi^r_{qsf} + \psi^r_{qsh}\right) sign\left(v^*_{inj}\right) I_h \cos\theta_{Ih}\right\} + \frac{3}{2}\frac{P}{2}\left(\psi^r_{dsh} i^r_{qsf} - \psi^r_{qsh} i^r_{dsf}\right)$$
$$\approx \frac{3}{2}\frac{P}{2} sign\left(v^*_{inj}\right) I_h \left\{\psi^r_{dsf} \sin\theta_{Ih} - \psi^r_{qsf} \cos\theta_{Ih}\right\}. \tag{15}$$

Notably, the flux linkage at the current operating point is required to calculate the HF torque. And it can be obtained from the flux table or the flux saturation model [10]-[11] using a standstill sensorless self-identification method [12].

The HF torque ripple varies according to the HF current vector angle $\sin\theta_{Ih}$, which means the HF torque could be minimized or maybe zero by regulating the HF current vector angle. Since the HF current vector angle change according to the voltage signal injection angle, the HF torque suppression can be achieved by adjusting the signal injection angle.

C. Proposed torque ripple suppression regulator

Fig. 5 presents the HF torque ripple according to the signal injection angle. The HF torque becomes zero if the voltage signal injection angle is about 0.4 rad. Mathematically, the signal injection angle can be calculated using the induced HF current angle as

$$\theta_{vh} = \tan^{-1}\left(\frac{L_{qsh}}{L_{dsh}} \tan\theta_{Ih}\right). \tag{16}$$

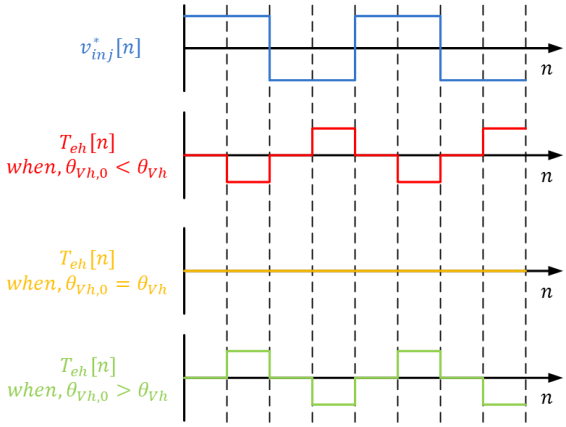

Fig. 6. High-frequency torque ripple according to the signal injection angle.

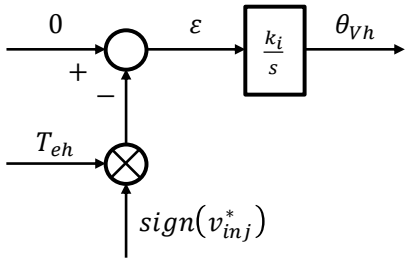

Fig. 7. Proposed HF torque suppression controller.

To minimize the HF torque ripple, the signal injection angle should be changed according to the HF torque ripples. For example, the signal injection angle should be increased if the HF torque ripple is negative or decreased when the HF torque ripple has a positive value. For that, the timing should be considered since the square-wave HF voltage signal is injected alternatively.

Fig. 6 presents the HF torque ripple according to the signal injection angle, where v^*_{inj} is the injection voltage signal, and $\theta_{Vh,0}$ is the voltage signal injection angle when the HF torque ripple is zero. The dashed line indicates the sampling point. The HF torque occurs if the signal injection angle error $\tilde{\theta}_{Vh} \equiv \theta_{Vh} - \theta_{Vh,0}$ is not zero. The HF torque alternates according to the injection signal and the sign of the injection angle error. For example, the HF torque is zero or negative when the injection voltage signal is V_h if the injection angle error is positive. If the injection angle error is negative, the HF torque is zero or positive when the injection voltage signal is $-V_h$.

Fig. 7 presents the proposed HF torque suppression controller. An integral controller is used to remove the HF torque ripple, and the error signal ε is determined according to the calculated HF torque and the injection voltage signal sign. Here, k_i is the controller's gain, determining the control performance. The torque ripple can be zero by adjusting the signal injection angle.

III. Verification Results

The proposed method was verified on an 11 kW IPMSM. Fig. 8 presents the experimental setup, consisting of an 11 kW interior permanent-magnet synchronous machine (IPMSM) and an 11 kW induction machine (IM), load machine. Table I show the nominal parameters of the test machine, and Table II presents the flux saturation model parameters used for experiments, where the model is shown in a. The proposed algorithm was implemented on a DSP TMS320F28377S. The switching and sampling frequencies were 5 kHz and 10 kHz, respectively. The square-wave HF voltage signal was 60 V/2.5 kHz, where the DC link voltage was 311 V.

Fig. 8. Experimental setup; 11 kW MG-set.

TABLE I
NOMINAL PARAMETERS OF 11 KW IPMSM

Content	Value
Rated power	11 kW
Rated voltage	184 V_{rms}
Rated current	39.5 A_{rms}
Pole number	6
Phase resistance	0.14 Ω
d-axis inductance	3.6 mH
q-axis inductance	4.3 mH
PM flux-linkage	0.26 Vs

TABLE II
IDENTIFIED FLUX SATURATION MODEL PARAMETERS OF 11 KW IPMSM

Parameter	Value	Parameter	Value
S	5.8	T	3.4
U	0	V	0
a_{d0}	294.1	a_{q0}	170.1
a_{dd}	4861.3	a_{qq}	3124.2
a_{dq}	443.8	i_f	77.4

Fig. 9 presents the performance of the proposed HF torque suppression control. The test machine controlled the rotor speed at 200 r/min while the load condition was changed from zero to the rated torque (60 Nm) by the load machine. The rotor position was measured by an encoder for a sensored control of the test machine. The HF voltage signal was injected to verify the proposed method, not for sensorless control. The signal injection angle θ_{vh}, calculated HF torque T_{eh}, load torque T_l, and the rotor speed ω_r are included in this figure.

Fig. 9(a) shows the results with the conventional method. The injection angle was maintained at zero, which means the signal was injected into the d-axis. It is observed that the HF torque increased with the increased load conditions. Under the rated load condition, the HF torque was about 1.5 Nm, which is 2.5% of the rated torque. Fig. 9(b) shows the results of the proposed method. The proposed HF torque suppression controller changed the signal injection angle to minimize the HF torque. As a result, the HF torque was significantly reduced. The HF torque under the rated load condition was only 0.3 Nm, which is only 20% of the conventional method.

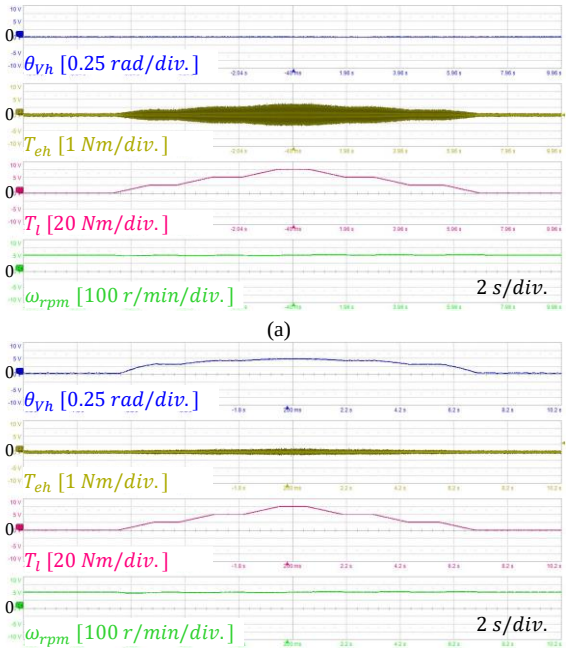

Fig. 9. Performance of the proposed method; (a) without the proposed method, and (b) with the proposed method.

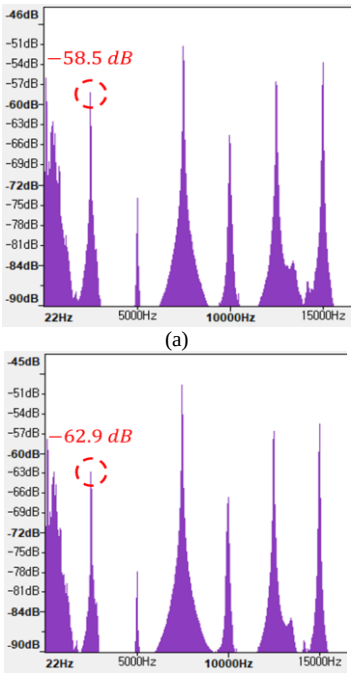

Fig. 10. Auditory noise measurement results; (a) without the proposed method, and (b) with the proposed method.

Fig. 10 shows the auditory noise measurement results at 200 r/min under the rated load condition. The signal injection sensorless control was used for the experiments. The auditory noise was measured using the "Blue Yeti Nano" microphone [13], and the results was analyzed using an "Audacity" program [14]. The result with the conventional method is shown in Fig. 10(a). The auditory noise at the injection signal frequency was -58.5 dB due to the generated HF torque from the induced HF current. However, the noise was reduced to -62.9 dB with the proposed method, as shown in Fig. 10(b).

IV. Conclusions

This paper proposes an HF torque suppression technique of the HF signal injection-based sensorless control. The HF torque occurs due to the HF current if the HF voltage signal is injected for sensorless control. This paper analyzes the HF torque considering the flux and current, including the fundamental and high frequencies. Furthermore, this paper proposes an HF torque suppression controller to minimize the HF torque ripple. Using an 11 kW IPMSM, experiments were performed to verify the proposed method, and the results proved that the proposed method could minimize the HF torque with the proposed method, resulting in reduced auditory noise.

Appendix

The magnetic flux saturation model of PMSMs was proposed in [10], where the model is

$$\begin{cases} i_{ds}^r = \left(a_{d0} + a_{dd}|\psi_{ds}^r|^S + \frac{a_{dq}}{V+2}|\psi_{ds}^r|^U|\psi_{qs}^r|^{V+2}\right)\psi_{ds}^r - i_f \\ i_{qs}^r = \left(a_{q0} + a_{qq}|\psi_{qs}^r|^T + \frac{a_{dq}}{U+2}|\psi_{ds}^r|^{U+2}|\psi_{qs}^r|^V\right)\psi_{qs}^r \end{cases}$$

References

[1] S. Ogasawara and H. Akagi, "An approach to position sensorless drive for brushless dc motor," *IEEE Trans. Ind. Appl.*, vol. 27, no. 5, pp. 928–933, Sep./Oct. 1991.

[2] S. Morimoto, K. Kawamoto, M. Sanada and Y. Takeda, "Sensorless control strategy for salient-pole PMSM based on extended EMF in rotating reference frame," in *IEEE Transactions on Industry Applications*, vol. 38, no. 4, pp. 1054-1061, July-Aug. 2002.

[3] Ji-Hoon Jang, Seung-Ki Sul, Jung-Ik Ha, K. Ide and M. Sawamura, "Sensorless drive of surface-mounted permanent-magnet motor by high-frequency signal injection based on magnetic saliency," in *IEEE Transactions on Industry Applications*, vol. 39, no. 4, pp. 1031-1039, July-Aug. 2003.

[4] Y. D. Yoon, S. K. Sul, S. Morimoto, and K. Ide, "High-bandwidth sensorless algorithm for AC machines based on square wave-type voltage injection," *IEEE Trans. Ind. Appl.*, vol. 47, pp. 1361-1370, May/Jun. 2011.

[5] P. Mattavelli, L. Tubiana and M. Zigliotto, "Torque-ripple reduction in PM synchronous motor drives using repetitive current control," in *IEEE Transactions on Power Electronics*, vol. 20, no. 6, pp. 1423-1431, Nov. 2005.

[6] Y. Xu, N. Parspour and U. Vollmer, "Torque Ripple Minimization Using Online Estimation of the Stator Resistances With Consideration of Magnetic Saturation," in *IEEE Transactions on Industrial Electronics*, vol. 61, no. 9, pp. 5105-5114, Sept. 2014.

[7] K. Kim, "A Novel Method for Minimization of Cogging Torque and Torque Ripple for Interior Permanent Magnet Synchronous Motor," in *IEEE Transactions on Magnetics*, vol. 50, no. 2, pp. 793-796, Feb. 2014, Art no. 7019604.

[8] K. Y. Hwang, J. H. Jo and B. I. Kwon, "A Study on Optimal Pole Design of Spoke-Type IPMSM With Concentrated Winding for Reducing the Torque Ripple by Experiment

Design Method," in *IEEE Transactions on Magnetics*, vol. 45, no. 10, pp. 4712-4715, Oct. 2009.
[9] Z. Lin, X. Li, Z. Wang, T. Shi and C. Xia, "Minimization of Additional High-Frequency Torque Ripple for Square-Wave Voltage Injection IPMSM Sensorless Drives," in *IEEE Transactions on Power Electronics*, vol. 35, no. 12, pp. 13345-13355, Dec. 2020.
[10] H. A. A. Awan, Z. Song, S. E. Saarakkala, and M. Hinkkanen, "Optimal torque control of saturated synchronous motors: Plug-and-play method," *IEEE Trans. Ind. Appl.*, vol. 54, no. 6, pp. 6110–6120, Nov./Dec. 2018.
[11] T. -G. Woo, S. -W. Park, S. -C. Choi, H. -J. Lee and Y. -D. Yoon, "Flux Saturation Model Including Cross Saturation for Synchronous Reluctance Machines and Its Identification Method at Standstill," in *IEEE Transactions on Industrial Electronics*, vol. 70, no. 3, pp. 2318-2328, March 2023.
[12] H. -J. Lee, J. -E. Joo and Y. -D. Yoon, "Standstill Sensorless Self-Commissioning Strategy of Synchronous Machine Considering Rotor Rotation Reduction Technique," *2022 International Power Electronics Conference (IPEC-Himeji 2022- ECCE Asia)*, Himeji, Japan, 2022, pp. 2694-2700.
[13] Microphone, Blue Yeti Nano, Logitech.
[14] Record program, Audacity, Audacity®